ACSNANO

www.acsnano.org

ARTICLE

Efficient Fabrication of High-Quality Single-Walled Carbon Nanotubes and Their Macroscopic Conductive Fibers

Xinyu Jiao, Chao Shi, Yiming Zhao, Lele Xu, Shaokang Liu, Peng-Xiang Hou,* Chang Liu,* and Hui-Ming Cheng

Cite This: *ACS Nano* 2022, 16, 20263–20271

Read Online

ACCESS | Metrics & More | Article Recommendations | Supporting Information

ABSTRACT: **High-purity and well-graphitized single-walled carbon nanotubes (SWCNTs) with excellent physiochemical properties are ideal building blocks for the assembly of various CNT macrostructures for a wide range of applications. We report the preparation of high-quality SWCNTs on a large scale using a floating catalyst chemical vapor deposition (FCCVD) method. Under the optimum conditions, the conversion rate of the carbon source to SWCNTs reached 28.8%, and 20.4% of the metal nanoparticles were active for SWCNT growth, which are 15% and ~400 times higher than those previously reported for FCCVD synthesis, respectively. As a result, the prepared SWCNTs have a very low residual catalyst content of ~1.9 wt % and a high rapid oxidation temperature of 717 °C. Using these high-quality SWCNTs, we spun macroscopic SWCNT fibers by a wet-spinning process. The resulting fibers had a high electrical conductivity of 6.67 MS/m, which is 32% higher than the best value previously reported for SWCNT fibers.**

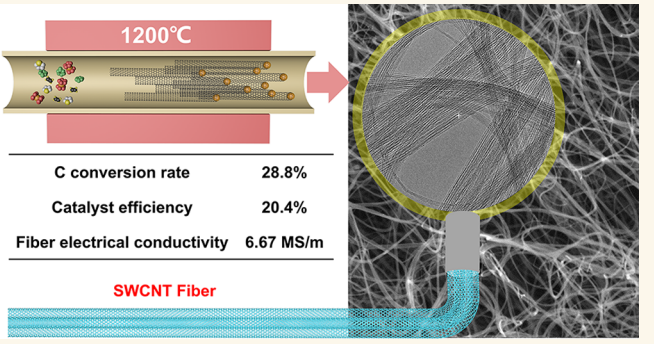

KEYWORDS: *single-walled carbon nanotubes, high quality, carbon conversion rate, catalyst efficiency, electrical conductivity, fiber*

Single-walled carbon nanotubes (SWCNTs) have attracted intense research interest due to their unique one-dimensional tubular structure and extraordinary physical and chemical properties.[1] The experimentally measured Young's modulus and tensile strength of SWCNTs have reached 1470 and 45 GPa, respectively.[2] With an electrical conductivity of ~10^7 S m^{-1} [3] and ultrahigh current-carrying capability several orders of magnitude higher than that of copper, SWCNTs are highly attractive for use in electrical conduction. The thermal conductivity of individual SWCNTs has been measured to be over 2000 W m^{-1} K^{-1},[4] about 5 times that of copper at room temperature. In addition, the density of SWCNTs is only approximately one-seventh that of copper, making them very promising for lightweight, high-strength, and highly conductive fiber applications.[5] To fabricate high-performance macroscopic SWCNT fibers, it is essential to efficiently obtain high-purity, well-graphitized SWCNT raw materials on a large scale.

Floating catalyst chemical vapor deposition (FCCVD) is a continuous, scalable, and cost-effective technique for SWCNT production.[6] Different from the traditional supported CVD technique, in a typical FCCVD process catalyst precursors are decomposed to form nanoparticles that float in the reactor and catalyze the growth of SWCNTs. Such floating catalysts have a good contact with the surrounding gas-phase carbon precursors, and therefore, a very high growth efficiency is expected. However, there is usually a considerable amount of residual catalyst (usually >10 wt %) remaining in the prepared SWCNT samples, and the reported carbon conversion rates have been very low, ranging from 0.9% to 9%,[7,8] which indicates that most of the carbon source gas passes through the reactor along with the carrier gas[9] or is converted to byproducts. It is therefore highly desirable to increase the carbon conversion rate and to minimize the content of residual catalyst and amorphous carbon impurities, so that high-quality SWCNTs are produced more efficiently.

Quite a few growth parameters, including temperature,[10] carrier gas,[11] carbon source,[12] growth promoter,[13] and catalyst

Received: June 15, 2022
Accepted: December 5, 2022
Published: December 7, 2022

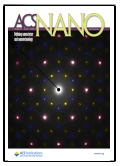

https://doi.org/10.1021/acsnano.2c05876
ACS Nano 2022, 16, 20263–20271

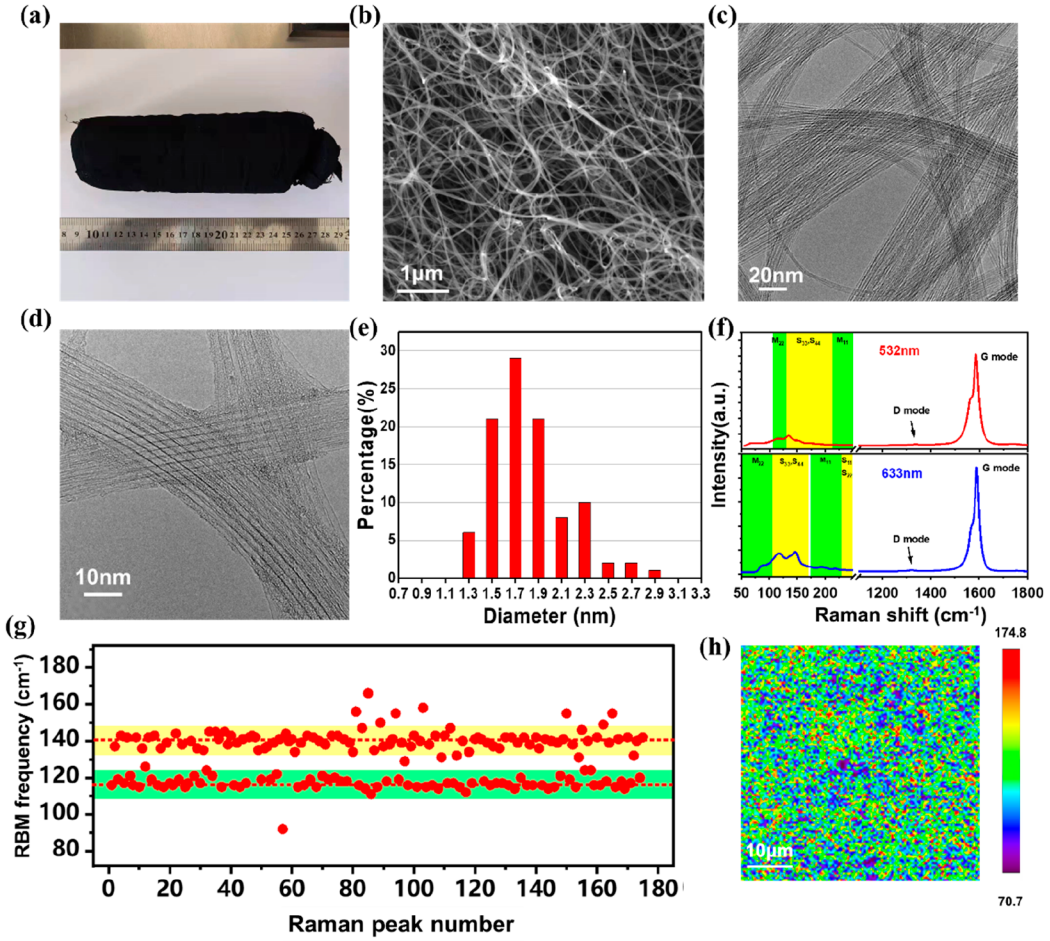

Figure 1. Structural characterization of SWCNT-1200. (a) Optical image of the SWCNTs. Typical (b) SEM and (c, d) TEM images of the sample. (e) Diameter distribution of the SWCNTs measured from 100 SWCNTs by TEM observation. (f) Raman spectra excited with 532 and 633 nm lasers. (g) Raman RBM frequency distribution (633 nm). (h) I_G/I_D map of an area of 50 × 50 μm^2 measured with a step of 400 nm.

precursor,[14] have been reported to affect the growth of SWCNTs by FCCVD. In this study, we used ferrocene and thiophene as the catalyst precursor and growth promoter, respectively, and C_2H_4 as the primary carbon source. A stable and accurate feed of the ferrocene and thiophene was achieved using an injection technique.[15] H_2 was used as a carrier gas to etch the amorphous carbon deposited on the catalyst particles, so that a longer lifetime of the catalysts was achieved.[16] We systematically investigated the effect of growth temperature on the rate of carbon conversion, the efficiency of catalysts, and the quality of SWCNTs obtained. Under the optimized growth conditions, the carbon conversion rate and catalyst efficiency reached 28.8% and 20.4%, respectively, which are both the highest values ever reported. The SWCNTs had a very low metallic impurity content of ∼1.9 wt % and a very high rapid oxidation temperature of 717 °C, due to their high purity and high degree of graphitization. Using these high-quality SWCNTs as a raw material, we fabricated SWCNT fibers by a wet-spinning process. The resulting long SWCNT fibers had a high electrical conductivity of 6.67 MS m^{-1}.

RESULTS AND DISCUSSION

Figure 1a shows an optical image of SWCNTs grown at 1200 °C that have aggregated to form a cotton-like mass. Figure 1b shows a typical SEM image of the as-prepared SWCNT-1200 sample; a network of SWCNT bundles with diameters of tens of nanometers is clearly seen. Typical TEM images in Figure 1c,d show that the tube walls are well-resolved and little residual catalyst is observed. Based on the measurements of 100 isolated SWCNTs by TEM, a diameter distribution is shown in Figure 1e. We can see that ∼90% have diameters in the range 1.5−2.3 nm. Multiwavelength Raman spectra of the SWCNTs are shown in Figure 1f. The RBM peaks originating from metallic and semiconducting SWCNTs are highlighted according to the Kataura plot.[17] Both metallic and semiconducting nanotube-related peaks are detected, indicating that the product is a mixture of metallic and semiconducting SWCNTs. The RBM peaks excited by both 633 and 532 nm are narrowly distributed in the range 110−146 cm^{-1}. The frequency distribution of 175 Raman RBM peaks excited with 633 nm irradiation is shown in Figure 1g, where we can see that more than 90% of the peaks are distributed in the ranges 140 ± 8 and 116 ± 6 cm^{-1}. We calculated the diameter (d) distribution of the SWCNTs using the formula $\omega = 218.3/d + 15.9$, where ω is the peak frequency,[18] and the results (1.7−2.2 nm) are in good agreement with those from TEM observations. The G-band peak shown in Figure 1f is very sharp and intense, while the D-band peak is almost invisible. Quantitatively, the intensity ratio of G to D bands (I_G/I_D) reached 142, indicating a high degree of graphitization of the

https://doi.org/10.1021/acsnano.2c05876
ACS Nano 2022, 16, 20263−20271

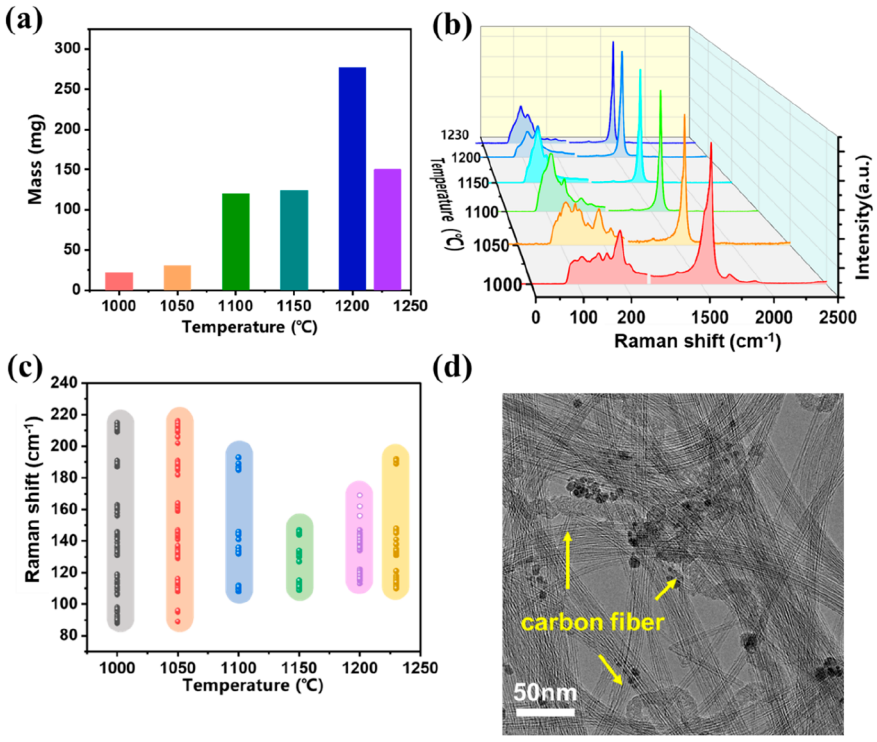

Figure 2. (a) Dependence of the yield of SWCNTs on growth temperature. (b) Raman spectra (excited with 633 nm) of the SWCNTs synthesized at different temperatures. (c) RBM frequency (633 nm) distribution from 30 points of each sample. (d) Typical TEM image of SWCNT-1230.

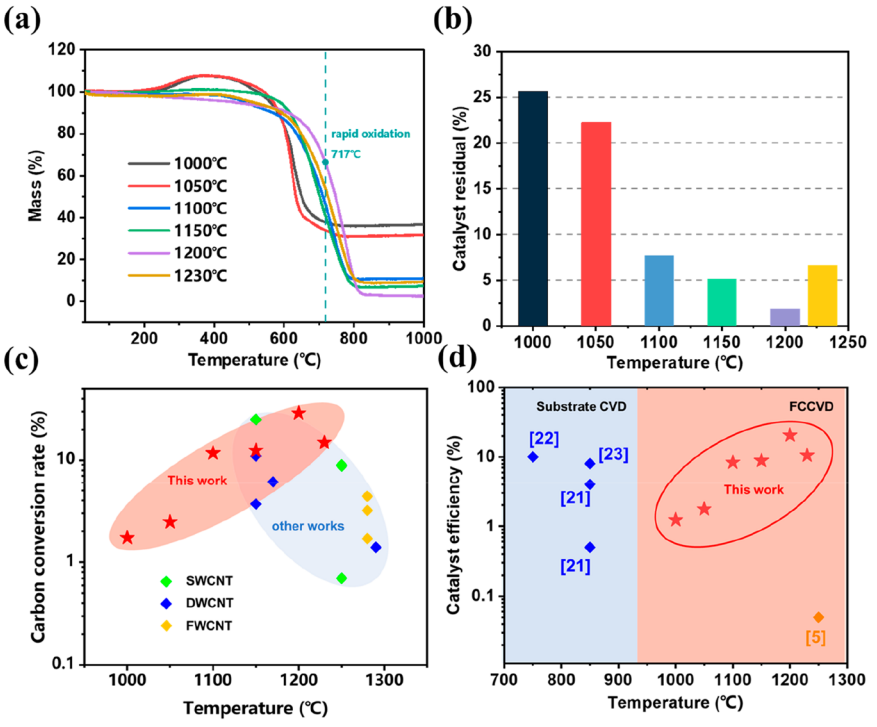

Figure 3. (a) Representative TG curves and (b) content of the residual catalyst of the SWCNTs synthesized at different temperatures. Comparison of the (c) carbon conversion rate[5,20] and (d) catalytic efficiency of this study with those of a previous report.

SWCNTs. To confirm the uniformity of the SWCNT sample, an I_G/I_D map was produced in an area of 50 × 50 μm^2 with steps of 400 nm (Figure 1h). The SWCNT sample shows I_G/I_D ratios ranging from 70.7 to 174.8 with an average value of 114 (Figure 1h and Figure S1), indicating the high overall quality of the sample. These highly pure and well-graphitized SWCNTs would be an ideal material for the fabrication of macroscopic conductive fibers.

https://doi.org/10.1021/acsnano.2c05876
ACS Nano 2022, 16, 20263−20271

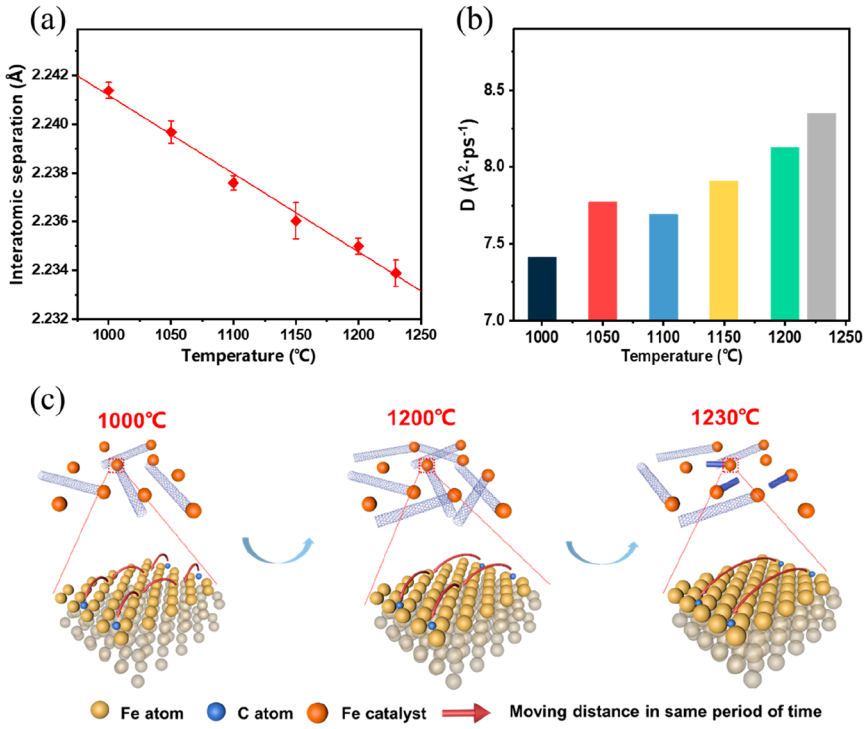

Figure 4. (a) Dependence of temperature on the Fe interatomic separation. (b) Carbon diffusion coefficients at different temperatures. (c) Illustration of the diffusion of carbon atoms in a Fe catalyst at 1000, 1200, and 1230 °C.

We studied the effect of growth temperature on the yield of SWCNTs. Optical images of the SWCNTs synthesized at 1000, 1050, 1100, 1150, 1200, and 1230 °C are shown in Figure S2. The yield of SWCNTs first increased with increasing growth temperature and reached a maximum of 277 mg h^{-1} (Figure 2a) at 1200 °C and then decreased at 1230 °C. Figure 2b shows Raman spectra (excited with a 633 nm laser) of the SWCNTs grown at different temperatures. The I_G/I_D intensity ratios increased from 63 (SWCNT-1000) to 142 (SWCNT-1200) and then decreased to 126 for SWCNT-1230. In Figure 2c, we show the frequency distribution of 30 RBM peaks for each SWCNT sample synthesized at different temperatures. It can be seen that SWCNT-1150 and SWCNT-1200 have the narrowest diameter distribution. There might be some correlation between the higher yield and narrower diameter distribution of these two samples, although this needs further investigation.

TEM observations (Figure S3) show that the samples synthesized at temperatures ≤1200 °C are composed of SWCNTs. However, for the sample grown at 1230 °C, carbon fibers (CFs, Figure 2d) and double-walled CNTs (DWCNTs, Figure S3f) coexist with SWCNTs. An enlarged typical RBM Raman spectrum of SWCNT-1230 (Figure S4) shows two separate groups of peaks centered at 63−156 and 199−226 cm^{-1}, which may be due to the outer and inner tube walls of the DWCNTs,[19] respectively.

We also investigated the effect of growth temperature on the carbon conversion rate (η_c) and catalyst efficiency. The former is defined as the molar ratio of produced SWCNTs (n_{CNT}) to the total carbon source (n_{total}) fed into the system.[5] The masses of SWCNT product (M_{CNT}) and carbon source introduced are normalized for 1 h. The value of M_{CNT} is calculated by subtracting the residual metal catalyst as found by TG analysis (Figure 3a) from the total yield of SWCNTs. The details of carbon conversion rate calculations are presented in the Supporting Information. The SWCNT-1200 sample shows the highest rapid oxidation temperature of 717 °C (at which the rate of weight loss reaches the maximum) and the lowest residual catalyst (Figure 3b), due to its high degree of graphitization and high purity. In addition, the calculated carbon conversion rate reached 28.8% (Figure 3c), ∼15% higher than that reported previously.[20]

The catalyst efficiency is defined as the percentage of the catalyst that grows SWCNTs: i.e., the active catalyst. The calculated values from this study together with those reported previously are shown in Figure 3d. The blue symbols show the catalyst efficiencies of Fe and Ni nanoparticles deposited on substrates, which were reported to be in the range of 0.4−10%,[21−23] obtained by directly observing the percentage of catalyst that grew CNTs. For the FCCVD method, Reguero et al.[7] reported a catalyst efficiency of ∼0.05%, as shown by the orange symbol in Figure 3d. They assessed the catalyst efficiency by assuming that the diameter of the catalyst is equal to that of the grown CNTs. The total mass of catalyst was calculated using TG, and the mass of active catalyst was calculated by the diameter, length, and density of SWCNTs. In fact, for FCCVD the catalyst size is generally much larger than the diameter of the SWCNTs. As shown in Figure S3, the catalyst size is not uniform, and the size distribution measured from a TEM image is shown in Figure S5b. We used an average diameter of 8.5 nm as the catalyst particle diameter. The Fe catalyst efficiency η_{Fe} was calculated based on Fe nanoparticle size, SWCNT diameter, and SWCNT length. The detailed calculations are given in the Supporting Information. It is seen that SWCNT-1200 has the highest catalyst efficiency of 20.4%.

The growth temperature may influence the synthesis of SWCNTs in multiple ways. For example, carbon source

https://doi.org/10.1021/acsnano.2c05876
ACS Nano 2022, 16, 20263−20271

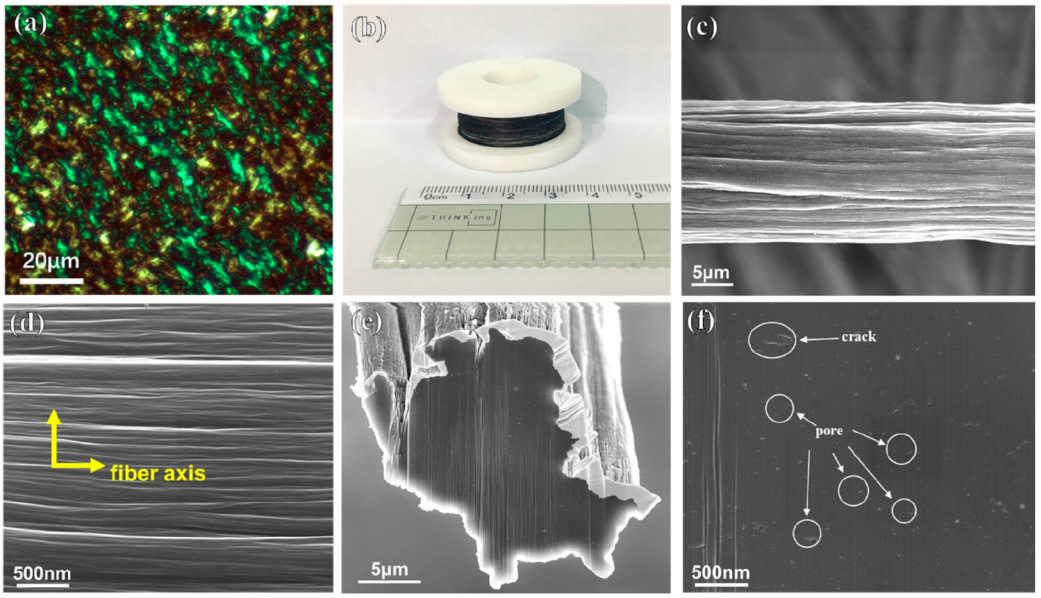

Figure 5. Characterization of SWCNT fibers prepared by wet spinning. (a) POM image of the SWCNT/CSA liquid crystal. (b) Optical image showing an ~20 m long SWCNT fiber wound on a PTFE roll. (c) Low-magnification and (d) high-magnification SEM images of the surface of a SWCNT fiber. (e) Low-magnification and (f) high-magnification SEM images of the cross section of a SWCNT fiber.

decomposition, aggregation and ripening of the catalyst, and carbon diffusion rate are all related to the growth temperature. In this work, however, the decomposition temperature of C_2H_4 and toluene is far below 1200 °C. In addition, the size of catalyst nanoparticles does not show an obvious increase with the increase of growth temperature (Figures S3 and S5), possibly because that the aggregation of Fe nanoparticles is also related to their interaction with carbon and the nucleation and growth of SWCNTs. Therefore, we focus more on the influence of temperature on the carbon diffusion rate.

To understand how temperature influences the carbon diffusion rate, we used molecular dynamics to simulate the Fe interatomic separation and carbon diffusion rate. A previous study[24] has shown that the Fe nanoparticles are liquefied at over 1000 °C; therefore, we based our simulation on a liquid Fe catalyst particle. Figure 4a and Figure S6 show that the interatomic separation decreases linearly from 2.241 to 2.233 Å when the temperature increases from 1000 to 1230 °C. This is because Fe atoms vibrate at their equilibrium position, and the vibration amplitude increases at higher temperatures, leading to a smaller interatomic separation.

The calculated carbon diffusion coefficients at different temperatures are shown Figure 4b. They tend to increase with increasing temperature, which would lead to a higher growth rate and yield of SWCNTs at higher temperatures. However, our results show a maximum yield at 1200 °C. Combined with simulation results, we take 1000, 1200, and 1230 °C as examples to elucidate the influence of temperature on the yield of SWCNTs, as shown in Figure 4c. We attribute the result to the coupling effect of Fe interatomic separation and carbon diffusion coefficient. The decreased Fe interatomic separation leads to a higher barrier for carbon atom diffusion in the Fe catalyst during the SWCNT growth, while the increased temperature provides a higher diffusion driving force. The high diffusion driving force overcomes the barrier of Fe interatomic separation, resulting in a higher diffusion rate at higher temperature and, hence, a higher SWCNT yield. To elucidate the abnormal yield decrease for SWCNT-1230, we characterized the microstructure of this sample under TEM. Figure S7 shows some short CNFs and Fe nanoparticles wrapped with amorphous carbon, which means that excess carbon has been provided because of the high diffusion rate, which leads to the growth of CNFs with much larger diameters, catalyst poisoning, and a decreased SWCNT yield. Therefore, we believe that an important reason for the maximum SWCNT yield at 1200 °C is that the growth rate of SWCNTs increases at higher temperature, due to the higher carbon concentration and faster carbon diffusion rate.

Macroscopic SWCNT fibers were prepared by a wet-spinning method,[25] and a schematic showing the spinning process is shown in Figure S8. Different from the previously reported wet-spinning method, the acid-washing step to remove residual catalyst is omitted in this study due to the high purity and very low metal impurity content in our raw SWCNTs. The liquid crystal solution of SWCNTs dispersed in CSA by protonation with a concentration of 1.6 wt % is anisotropic under cross-polarized light (Figure 5a). It was extruded through a spinneret (180 μm diameter) at a rate of 0.07 mL/min into an acetone coagulant bath to form macroscopic SWCNT fibers. The spun SWCNT fibers were then wound on a PTFE roll (Figure 5b) and dried at 110 °C for 24 h. The density of the fibers was measured to be 1.3 g cm^{-3}.

SEM images showing the morphology of the obtained SWCNT fibers are shown in Figure 5c and Figure S9. The fiber has a uniform diameter of ~16 μm, and a high-magnification image (Figure 5d) shows that the individual SWCNTs are highly aligned along the axis of the fiber. SEM observation of the cross section (Figure 5e) verified the high packing density of the SWCNTs. At higher magnification, some sub-micrometer pores and cracks were seen in the fiber (Figure 5f), which can be attributed to the nonuniform shrinkage of the SWCNT fiber when the liquid crystal solution is extruded into the coagulant bath. A TG curve of SWCNT fibers is shown in Figure S10. We can see that the oxidation temperature

https://doi.org/10.1021/acsnano.2c05876
ACS Nano 2022, 16, 20263−20271

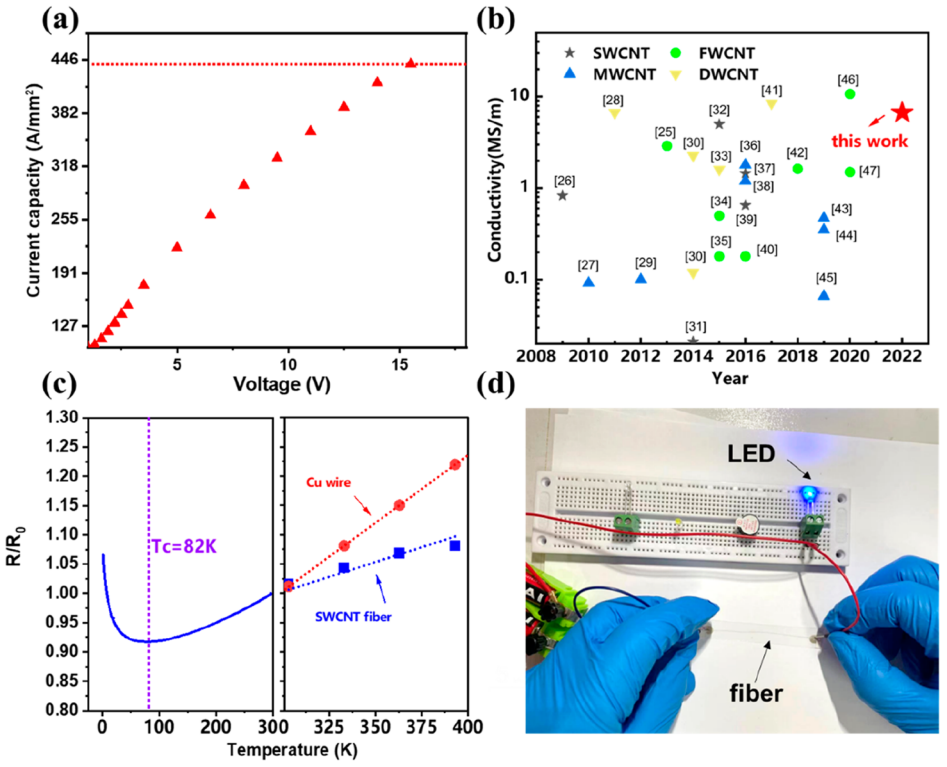

Figure 6. (a) Current capacity of a SWCNT fiber. (b) Comparison of the previously reported electrical conductivities of CNT fibers together with our result. (c) Temperature dependence of fiber relative resistance. (d) Illumination of an LED connected with a 5 cm long SWCNT fiber.

becomes lower, possibly due to the defects introduced during the dispersion process of SWCNTs.

The electrical performance of the obtained SWCNT fibers was measured using a four-probe method. As shown in Figure 6a, a high current density of 445 A mm^{-2} was achieved and the average room-temperature electrical conductivity was 6.67 MS m^{-1}. The concentrations of SWCNT solution used for spinning SWCNT fibers in this study were in the range of 1.0−1.6 wt %, and the fibers spun from the 1.6 wt % solution showed the highest electrical conductivity (Figure S11). Figure 6b summarizes the previously reported electrical conductivities of CNT fibers prepared by wet- and dry-spinning methods for comparison with our fibers[25−47] (detailed data are given in Table S1). This shows that fibers fabricated using DWCNTs and few-walled carbon nanotubes (FWCNTs) show the highest electrical conductivity, possibly because the functionalization of nanotubes during the dispersion process occurs only on the outer shell, while leaving the inner tubes intact.[48] Our SWCNT fiber shows the highest electrical conductivity compared to the previously reported SWCNT fibers, ∼32% higher than the best value of 5.0 MS m^{-1}. We also investigated the temperature-dependent resistance of our SWCNT fibers (Figure 6c). The resistance at 300 K is defined as R_0. We see that the resistivity decreases with increasing temperature in the range 4−82 K, showing semiconducting behavior. The behavior in this region was interpreted by carrier hopping or tunneling due to inter-SWCNT transport because electron−phonon scattering was weak but increased with increasing temperature. At T > 82 K, the resistivity increases with increasing temperature, a metallic behavior. The resistance of our SWCNT fibers and commercial Cu wires was measured at 300−400 K, which is the working temperature range of the latter (Figure 6c), from which the temperature coefficient of resistivity (TCR) was calculated. Our SWCNT fiber has a TCR value of 1.37 × 10^{-3} K^{-1}, which is 67% lower than that of Cu wire. Figure S12 shows that the tensile strength of the SWCNT fiber was 745 MPa with a maximum strain of 6.5%. We also assembled a simple circuit using a 5 cm long SWCNT fiber to replace partial copper wire, and a light-emitting diode was illuminated successfully (Figure 6d).

CONCLUSIONS

We have developed an injection-FCCVD method using ferrocene as the catalyst precursor, hydrogen as the carrier gas, and ethylene as the carbon source for the efficient synthesis of SWCNTs. At an optimum growth temperature of 1200 °C, the carbon conversion rate and catalyst efficiency were 28.8% and 20.4%, respectively, much higher than those reported previously. In addition, the prepared SWCNTs showed a very low residual catalyst content of ∼1.9 wt % and a high rapid oxidation temperature of 717 °C. Theoretical calculations indicate that the diffusion coefficient of carbon in an Fe catalyst, which is closely related to the growth temperature, plays an important role in determining the SWCNT growth rate and the synthesis efficiency. Using these high-purity and well-graphitized SWCNTs as a raw material, SWCNT fibers were fabricated by wet spinning. They had a high electrical conductivity of 6.67 MS m^{-1}, which is the highest reported value for SWCNT fibers.

EXPERIMENTAL METHODS

Preparation of High-Quality SWCNTs. An injection-FCCVD method[49,50] was used to synthesize SWCNTs and a schematic of the experimental setup is shown in Figure S13. A ceramic tube with a

https://doi.org/10.1021/acsnano.2c05876
ACS Nano 2022, 16, 20263−20271

diameter of 40 mm and length of 800 mm was inserted into a horizontal tubular furnace and used as a reactor. The furnace temperature was increased to the preset growth temperature under the protection of an Ar flow. A 4700 sccm amount of H_2 carrier gas and 8 sccm of the C_2H_4 carbon source were then introduced, and a mixed solution containing toluene, ferrocene, and thiophene (Fe:S molar ratio from 1 to 4), which serve as the liquid carbon source, the catalyst precursor, and growth promoter, respectively, was injected into the reactor using a syringe pump. The injection rate was ~0.6 mL h^{-1}. SWCNTs grew from Fe catalyst nanoparticles and were carried by the carrier gas to the low-temperature zone of the reactor. The growth time was set to be 1 h. We investigated the effect of synthesis temperature (1000, 1050, 1100, 1150, 1200, and 1230 °C) on the SWCNT growth efficiency and the quality of the SWCNTs, which are denoted as SWCNT-1000, SWCNT-1050, SWCNT-1100, SWCNT-1150, SWCNT-1200, and SWCNT-1230, respectively.

SWCNT Fiber Spinning. To prepare the SWCNT fibers, as-grown SWCNTs were mixed by a planet mixer (FlackTek SpeedMixer DAC150.1 FVZ-K) with 99% chlorosulfuric acid (CSA, Sigma-Aldrich) to form a spinnable liquid crystalline solution (Figure S14) whose concentration was 1.0~1.6 wt % and was characterized using a Leica DP2700M polarizing optical microscope (POM). It was then extruded through a needle with an inner diameter of 180 μm into an acetone coagulating bath at an injection rate of 0.07 mL/min. The fibers obtained were exposed to air to volatize residual acetone and then wound on a rotating roller with an outer diameter of 19 mm, whose rotation speed could be adjusted in the range of 0−300 rpm.

Characterization of the SWCNTs and Fibers. The SWCNT samples were characterized using a WITec Alpha 300R Raman spectrometer with 633 and 532 nm lasers. A NETZSCH STA449F5 thermal gravimetric analyzer (TGA) was used to characterize the purity and oxidization resistance of the SWCNTs. A FEI Verios G4 scanning electron microscope (SEM) and Tecnai G2 F20 (operated at 200 kV) transmission electron microscope (TEM) were used to examine the morphology and microstructure of the samples. A four-point probe connected to a Keithley 2401 source meter was used to measure the electrical resistance of SWCNT fibers. To reduce the measurement error of fiber diameter, we randomly cut several 5 cm long fibers from an ~30 m long fiber. Five points in each fiber were randomly chosen to measure the diameter under SEM. We used the average value of these measured diameters to calculate the electrical conductivity of the fiber.

ASSOCIATED CONTENT

Supporting Information

The Supporting Information is available free of charge at https://pubs.acs.org/doi/10.1021/acsnano.2c05876.

Details of the four-probe method, estimation of SWCNT length, and calculation of carbon conversion rate and catalyst efficiency (PDF)

AUTHOR INFORMATION

Corresponding Authors

Peng-Xiang Hou − *Shenyang National Laboratory for Materials Science, Institute of Metal Research, Chinese Academy of Sciences, Shenyang 110016, People's Republic of China; School of Materials Science and Engineering, University of Science and Technology of China, Hefei 230026, People's Republic of China*; Email: pxhou@imr.ac.cn

Chang Liu − *Shenyang National Laboratory for Materials Science, Institute of Metal Research, Chinese Academy of Sciences, Shenyang 110016, People's Republic of China; School of Materials Science and Engineering, University of Science and Technology of China, Hefei 230026, People's Republic of China*; orcid.org/0000-0003-3016-3997; Email: cliu@imr.ac.cn

Authors

Xinyu Jiao − *Shenyang National Laboratory for Materials Science, Institute of Metal Research, Chinese Academy of Sciences, Shenyang 110016, People's Republic of China; School of Materials Science and Engineering, University of Science and Technology of China, Hefei 230026, People's Republic of China*

Chao Shi − *Shenyang National Laboratory for Materials Science, Institute of Metal Research, Chinese Academy of Sciences, Shenyang 110016, People's Republic of China*

Yiming Zhao − *Shenyang National Laboratory for Materials Science, Institute of Metal Research, Chinese Academy of Sciences, Shenyang 110016, People's Republic of China; School of Materials Science and Engineering, University of Science and Technology of China, Hefei 230026, People's Republic of China*

Lele Xu − *Shenyang National Laboratory for Materials Science, Institute of Metal Research, Chinese Academy of Sciences, Shenyang 110016, People's Republic of China; School of Materials Science and Engineering, University of Science and Technology of China, Hefei 230026, People's Republic of China*

Shaokang Liu − *Shenyang National Laboratory for Materials Science, Institute of Metal Research, Chinese Academy of Sciences, Shenyang 110016, People's Republic of China; School of Materials Science and Engineering, University of Science and Technology of China, Hefei 230026, People's Republic of China*

Hui-Ming Cheng − *Shenyang National Laboratory for Materials Science, Institute of Metal Research, Chinese Academy of Sciences, Shenyang 110016, People's Republic of China; Faculty of Materials Science and Engineering/Institute of Technology for Carbon Neutrality, Shenzhen Institute of Advanced Technology, Chinese Academy of Sciences, Shenzhen 518055, People's Republic of China*; orcid.org/0000-0002-5387-4241

Complete contact information is available at: https://pubs.acs.org/10.1021/acsnano.2c05876

Author Contributions

X.J. amd C.S. were equal major contributors to this work.

Notes

The authors declare no competing financial interest.

ACKNOWLEDGMENTS

This work was supported by the National Natural Science Foundation of China (Grants 52072375, 52130209, 51872293, 52188101), the Liaoning Revitalization Talents Program (XLYC2002037), and the Basic Research Project of the Natural Science Foundation of Shandong Province, China (ZR2019ZD49).

REFERENCES

(1) Madrona, C.; Vila, M.; Oropeza, F. E.; de la Peña O'Shea, V. A.; Vilatela, J. J. Macroscopic Yarns of $FeCl_3$-Intercalated Collapsed Carbon Nanotubes with High Doping and Stability. *Carbon.* **2021**, *173*, 311−321.

(2) Yu, M. F.; Files, B. S.; Arepalli, S.; Ruoff, R. S. Tensile Loading of Ropes of Single Wall Carbon Nanotubes and Their Mechanical Properties. *Phys. Rev. Lett.* **2000**, *84* (24), 5552−5555.

(3) Kong, J.; Zhou, C.; Morpurgo, A.; Soh, H. T.; Quate, C. F.; Marcus, C.; Dai, H. Synthesis, Integration, and Electrical Properties of Individual Single-Walled Carbon Nanotubes. *Appl. Phys. a-Mater.* **1999**, *69* (3), 305−308.
(4) Fujii, M.; Zhang, X.; Xie, H.; Ago, H.; Takahashi, K.; Ikuta, T.; Abe, H.; Shimizu, T. Measuring the Thermal Conductivity of a Single Carbon Nanotube. *Phys. Rev. Lett.* **2005**, *95* (6), 065502.
(5) Weller, L.; Smail, F. R.; Elliott, J. A.; Windle, A. H.; Boies, A. M.; Hochgreb, S. Mapping the Parameter Space for Direct-Spun Carbon Nanotube Aerogels. *Carbon.* **2019**, *146*, 789−812.
(6) Hou, P. X.; Zhang, F.; Zhang, L. L.; Liu, C.; Cheng, H. M. Synthesis of Carbon Nanotubes by Floating Catalyst Chemical Vapor Deposition and Their Applications. *Adv. Funct. Mater.* **2022**, *32* (11), 2108541.
(7) Reguero, V.; Aleman, B.; Mas, B.; Vilatela, J. J. Controlling Carbon Nanotube Type in Macroscopic Fibers Synthesized by the Direct Spinning Process. *Chem. Mater.* **2014**, *26* (11), 3550−3557.
(8) Hou, G. F.; Chauhan, D.; Ng, V.; Xu, C. H.; Yin, Z. Z.; Paine, M.; Su, R. T.; Shanov, V.; Mast, D.; Schulz, M.; et al. Gas Phase Pyrolysis Synthesis of Carbon Nanotubes at High Temperature. *Mater. Des.* **2017**, *132*, 112−118.
(9) Ingram, G.; Rizvi, S. M. H. The Pyrolytic Identification of Organic Molecules. *Microchem. J.* **1974**, *19* (3), 253−271.
(10) Li, H. B.; Page, A. J.; Irle, S.; Morokuma, K. Temperature Dependence of Catalyst-Free Chirality-Controlled Single-Walled Carbon Nanotube Growth from Organic Templates. *J. Phys. Chem. Lett.* **2013**, *4* (18), 3176−3180.
(11) LIU; Ren, J. X.; Duan, Z.; Xie, L. Y.; You-Chang. Effects of H_2O on Preparation of Single-Wall Carbon Nanotubes (SWCNT) by Catalytic Decomposition of CH_4 in Ar. *Acta Chim. Sinica.* **2004**, *62* (8), 775−782.
(12) Shukla, B.; Saito, T.; Ohmori, S.; Koshi, M.; Yumura, M.; Iijima, S. Interdependency of Gas Phase Intermediates and Chemical Vapor Deposition Growth of Single Wall Carbon Nanotubes. *Chem. Mater.* **2010**, *22* (22), 6035−6043.
(13) Suzuki, S.; Mori, S. The Role of Sulfur in Promoted Growth of Carbon Nanotubes in Chemical Vapor Deposition Proposed through the Characterizations on Catalytic Nanoparticles. *Appl. Surf. Sci.* **2019**, *471*, 587−594.
(14) Majeed, A.; Hou, P. X.; Zhang, F.; Tabassum, H.; Li, X.; Li, G. X.; Liu, C.; Cheng, H. M. A Freestanding Single-Wall Carbon Nanotube Film Decorated with N-Doped Carbon-Encapsulated Ni Nanoparticles as a Bifunctional Electrocatalyst for Overall Water Splitting. *Adv. Sci.* **2019**, *6* (12), 1802177.
(15) Li, W. S.; Hou, P. X.; Liu, C.; Sun, D. M.; Yuan, J.; Zhao, S. Y.; Yin, L. C.; Cong, H.; Cheng, H. M. High-Quality, Highly Concentrated Semiconducting Single-Wall Carbon Nanotubes for Use in Field Effect Transistors and Biosensors. *ACS Nano* **2013**, *7* (8), 6831−6839.
(16) Hou, P. X.; Li, W. S.; Zhao, S. Y.; Li, G. X.; Shi, C.; Liu, C.; Cheng, H. M. Preparation of Metallic Single-Wall Carbon Nanotubes by Selective Etching. *ACS Nano* **2014**, *8* (7), 7156−7162.
(17) Strano, M. S. Probing Chiral Selective Reactions Using a Revised Kataura Plot for the Interpretation of Single-Walled Carbon Nanotube Spectroscopy. *J. Am. Chem. Soc.* **2003**, *125* (51), 16148−16153.
(18) Endo, M.; Kim, Y. A.; Hayashi, T.; Muramatsu, H.; Terrones, M.; Saito, R.; Villalpando-Paez, F.; Chou, S. G.; Dresselhaus, M. S. Nanotube Coalescence-Inducing Mode: A Novel Vibrational Mode in Carbon Systems. *Small.* **2006**, *2* (8−9), 1031−1036.
(19) Ren, W. C.; Li, F.; Chen, J. A.; Bai, S.; Cheng, H. M. Morphology, Diameter Distribution and Raman Scattering Measurements of Double-Walled Carbon Nanotubes Synthesized by Catalytic Decomposition of Methane. *Chem. Phys. Lett.* **2002**, *359* (3−4), 196−202.
(20) Zhang, Q.; Zhou, W.; Xia, X.; Li, K.; Zhang, N.; Wang, Y.; Xiao, Z.; Fan, Q.; Kauppinen, E. I.; Xie, S. Transparent and Freestanding Single-Walled Carbon Nanotube Films Synthesized Directly and Continuously Via a Blown Aerosol Technique. *Adv. Mater.* **2020**, *32* (39), No. 2004277.
(21) Paillet, M.; Jourdain, V.; Poncharal, P.; Sauvajol, J. L.; Zahab, A.; Meyer, J. C.; Roth, S.; Cordente, N.; Amiens, C.; Chaudret, B. Versatile Synthesis of Individual Single-Walled Carbon Nanotubes from Nickel Nanoparticles for the Study of Their Physical Properties. *J. Phys. Chem. B* **2004**, *108* (44), 17112−17118.
(22) Ishida, M.; Hongo, H.; Nihey, F.; Ochiai, Y. Diameter-Controlled Carbon Nanotubes Grown from Lithographically Defined Nanoparticles. *Jpn. J. Appl. Phys., Part 2.* **2004**, *43* (10b), L1356−L1358.
(23) Paillet, M.; Jourdain, V.; Poncharal, P.; Sauvajol, J. L.; Zahab, A.; Meyer, J. C.; Roth, S.; Cordente, N.; Amiens, C.; Chaudret, B. Growth and Physical Properties of Individual Single-Walled Carbon Nanotubes. *Diamond Relat. Mater.* **2005**, *14* (9), 1426−1431.
(24) Moisala, A.; Nasibulin, A. G.; Kauppinen, E. I. The Role of Metal Nanoparticles in the Catalytic Production of Single-Walled Carbon Nanotubes—a Review. *J. Phys.: Condens. Matter.* **2003**, *15* (42), S3011−S3035.
(25) Behabtu, N.; Young, C. C.; Tsentalovich, D. E.; Kleinerman, O.; Wang, X.; Ma, A. W.; Bengio, E. A.; ter Waarbeek, R. F.; de Jong, J. J.; Hoogerwerf, R. E.; et al. Strong, Light, Multifunctional Fibers of Carbon Nanotubes with Ultrahigh Conductivity. *Science.* **2013**, *339* (6116), 182−186.
(26) Davis, V. A.; Parra-Vasquez, A. N.; Green, M. J.; Rai, P. K.; Behabtu, N.; Prieto, V.; Booker, R. D.; Schmidt, J.; Kesselman, E.; Zhou, W.; et al. True Solutions of Single-Walled Carbon Nanotubes for Assembly into Macroscopic Materials. *Nat. Nanotechnol.* **2009**, *4* (12), 830−834.
(27) Liu, K.; Sun, Y.; Lin, X.; Zhou, R.; Wang, J.; Fan, S.; Jiang, K. Scratch-Resistant, Highly Conductive, and High-Strength Carbon Nanotube-Based Composite Yarns. *ACS Nano* **2010**, *4* (10), 5827−5834.
(28) Zhao, Y.; Wei, J.; Vajtai, R.; Ajayan, P. M.; Barrera, E. V. Iodine Doped Carbon Nanotube Cables Exceeding Specific Electrical Conductivity of Metals. *Sci. Rep.* **2011**, *1*, 83.
(29) Liu, K.; Zhu, F.; Liu, L.; Sun, Y.; Fan, S.; Jiang, K. Fabrication and Processing of High-Strength Densely Packed Carbon Nanotube Yarns without Solution Processes. *Nanoscale.* **2012**, *4* (11), 3389−3393.
(30) Wang, J. N.; Luo, X. G.; Wu, T.; Chen, Y. High-Strength Carbon Nanotube Fibre-Like Ribbon with High Ductility and High Electrical Conductivity. *Nat. Commun.* **2014**, *5*, 3848.
(31) Jiang, C.; Saha, A.; Young, C. C.; Hashim, D. P.; Ramirez, C. E.; Ajayan, P. M.; Pasquali, M.; Marti, A. A. Macroscopic Nanotube Fibers Spun from Single-Walled Carbon Nanotube Polyelectrolytes. *ACS Nano* **2014**, *8* (9), 9107−9112.
(32) Bucossi, A. R.; Cress, C. D.; Schauerman, C. M.; Rossi, J. E.; Puchades, I.; Landi, B. J. Enhanced Electrical Conductivity in Extruded Single-Wall Carbon Nanotube Wires from Modified Coagulation Parameters and Mechanical Processing. *ACS Appl. Mater. Interfaces.* **2015**, *7* (49), 27299−27305.
(33) Guo, F. M.; Li, C.; Wei, J. Q.; Xu, R. Q.; Zhang, Z. L.; Cui, X.; Wang, K. L.; Wu, D. H. Fabrication of Highly Conductive Carbon Nanotube Fibers for Electrical Application. *Mater. Res. Express.* **2015**, *2* (9), 095604.
(34) Ryu, S.; Chou, J. B.; Lee, K.; Lee, D.; Hong, S. H.; Zhao, R.; Lee, H.; Kim, S. G. Direct Insulation-to-Conduction Transformation of Adhesive Catecholamine for Simultaneous Increases of Electrical Conductivity and Mechanical Strength of Cnt Fibers. *Adv. Mater.* **2015**, *27* (21), 3250−3255.
(35) Zhang, L.; Wang, X.; Xu, W.; Zhang, Y.; Li, Q.; Bradford, P. D.; Zhu, Y. Strong and Conductive Dry Carbon Nanotube Films by Microcombing. *Small.* **2015**, *11* (31), 3830−3836.
(36) Liu, P.; Hu, D. C. M.; Tran, T. Q.; Jewell, D.; Duong, H. M. Electrical Property Enhancement of Carbon Nanotube Fibers from Post Treatments. *Colloids Surf., A* **2016**, *509*, 384−389.
(37) Mukai, K.; Asaka, K.; Wu, X. L.; Morimoto, T.; Okazaki, T.; Saito, T.; Yumura, M. Wet Spinning of Continuous Polymer-Free

https://doi.org/10.1021/acsnano.2c05876
ACS Nano 2022, 16, 20263−20271

Carbon-Nanotube Fibers with High Electrical Conductivity and Strength. *Appl. Phys. Express.* **2016**, *9* (5), 055101.
(38) Tran, T. Q.; Fan, Z.; Liu, P.; Myint, S. M.; Duong, H. M. Super-Strong and Highly Conductive Carbon Nanotube Ribbons from Post-Treatment Methods. *Carbon.* **2016**, *99*, 407−415.
(39) Wu, X. L.; Morimoto, T.; Mukai, K.; Asaka, K.; Okazaki, T. Relationship between Mechanical and Electrical Properties of Continuous Polymer-Free Carbon Nanotube Fibers by Wet-Spinning Method and Nanotube-Length Estimated by Far-Infrared Spectroscopy. *J. Phys. Chem. C* **2016**, *120* (36), 20419−20427.
(40) Zhang, L. W.; Wang, X.; Li, R.; Li, Q. W.; Bradford, P. D.; Zhu, Y. T. Microcombing Enables High-Performance Carbon Nanotube Composites. *Compos. Sci. Technol.* **2016**, *123*, 92−98.
(41) Tsentalovich, D. E.; Headrick, R. J.; Mirri, F.; Hao, J.; Behabtu, N.; Young, C. C.; Pasquali, M. Influence of Carbon Nanotube Characteristics on Macroscopic Fiber Properties. *ACS Appl. Mater. Interfaces.* **2017**, *9* (41), 36189−36198.
(42) Wang, P.; Liu, D. D.; Zou, J. Y.; Ye, Y. H.; Hou, L.; Zhao, J. N.; Men, C. L.; Zhang, X. H.; Li, Q. W. Gas Infiltration of Bromine to Enhance the Electrical Conductivity of Carbon Nanotube Fibers. *Mater. Des.* **2018**, *159*, 138−144.
(43) Li, M.; Song, Y. H.; Zhang, C.; Yong, Z. Z.; Qiao, J.; Hu, D. M.; Zhang, Z. G.; Wei, H. Z.; Di, J. T.; Li, Q. W. Robust Carbon Nanotube Composite Fibers: Strong Resistivities to Protonation, Oxidation, and Ultrasonication. *Carbon.* **2019**, *146*, 627−635.
(44) Kim, Y. J.; Park, J.; Kim, H.; Jeong, H. S.; Lee, J. H.; Kim, S. M.; Kim, Y. K. Simultaneous Enhancement of Mechanical and Electrical Properties of Carbon Nanotube Fiber by Infiltration and Subsequent Carbonization of Resorcinol-Formaldehyde Resin. *Compos Part B-Eng.* **2019**, *163*, 431−437.
(45) Liang, X.; Gao, Y.; Duan, J.; Liu, Z.; Fang, S.; Baughman, R. H.; Jiang, L.; Cheng, Q. Enhancing the Strength, Toughness, and Electrical Conductivity of Twist-Spun Carbon Nanotube Yarns by Π Bridging. *Carbon.* **2019**, *150*, 268−274.
(46) Taylor, L. W.; Dewey, O. S.; Headrick, R. J.; Komatsu, N.; Peraca, N. M.; Wehmeyer, G.; Kono, J.; Pasquali, M. Improved Properties, Increased Production, and the Path to Broad Adoption of Carbon Nanotube Fibers. *Carbon.* **2021**, *171*, 689−694.
(47) Lee, S.-H.; Park, J.; Park, J. H.; Lee, D.-M.; Lee, A.; Moon, S. Y.; Lee, S. Y.; Jeong, H. S.; Kim, S. M. Deep-Injection Floating-Catalyst Chemical Vapor Deposition to Continuously Synthesize Carbon Nanotubes with High Aspect Ratio and High Crystallinity. *Carbon.* **2021**, *173*, 901−909.
(48) Bulmer, J. S.; Kaniyoor, A.; Elliott, J. A. A Meta-Analysis of Conductive and Strong Carbon Nanotube Materials. *Adv. Mater.* **2021**, *33* (36), No. 2008432.
(49) Jiang, S.; Hou, P. X.; Chen, M. L.; Wang, B. W.; Sun, D. M.; Tang, D. M.; Jin, Q.; Guo, Q. X.; Zhang, D. D.; Du, J. H.; et al. Ultrahigh-Performance Transparent Conductive Films of Carbon-Welded Isolated Single-Wall Carbon Nanotubes. *Sci. Adv.* **2018**, *4* (5), No. eaap9264.
(50) Hu, X. G.; Hou, P. X.; Liu, C.; Zhang, F.; Liu, G.; Cheng, H. M. Small-Bundle Single-Wall Carbon Nanotubes for High-Efficiency Silicon Heterojunction Solar Cells. *Nano Energy.* **2018**, *50*, 521−527.

https://doi.org/10.1021/acsnano.2c05876
ACS Nano 2022, 16, 20263−20271